分子間トンネル顕微鏡と分子探針

梅 澤 喜 夫*

Molecular Tips for "Intermolecular Tunneling Microscopy"

Yoshio Umezawa*

This is the third year of the Toyota fellow report. In this review, molecular tips for "intermolecular tunneling microscopy" is reported.

We describe herein the concept, principle, and experimental results of the molecular tips for chemically selective STM. It has been shown that molecular tips allow chemically selective imaging to recognize particular functional groups or chemical species based upon the hydrogen bond, metal coordination, and charge-transfer interactions between sample and tip molecules. The selectivity can be tailored upon designing functional groups of the tip molecules. Furthermore, the molecular tips were successfully applied to differentiate nucleobases. This technique may be coined "intermolecular tunneling microscopy" as its principle goes, and is of general significance for novel molecular imaging of chemical identities at the membrane and solid surfaces.

1. Introduction

Scanning tunneling microscopy (STM) offers real-space observation with extremely high spatial resolution and has been a powerful tool to study atoms/molecules adsorbed on conducting surfaces.[1-3] It is, however, often difficult to discriminate functional groups and chemical species from the conventional STM image contrast. We have studied on construction of molecular tips for STM. The molecular tips are prepared by chemical modification of underlying metal tips typically with self-assembled monolayers (SAMs) of thiols [Fig. 1(a)], and the outermost single adsorbate probes electron tunneling to or from a sample molecule. Importantly, the tunneling current increases when sample and tip molecules form chemical interactions that provide overlap of their electronic wave functions, that is, hydrogen bond,[4-8] metal-coordination bond,[9] and charge-transfer[10] interactions [Fig. 1(b)]. The current increase is ascribed to the facilitated tunneling through the overlapped wave functions. We have demonstrated that this phenomenon can be utilized for selective observation of chemical species to overcome poor chemical selectivity in conventional STM.

2011年1月24日 受理
*豊田理化学研究所フェロー

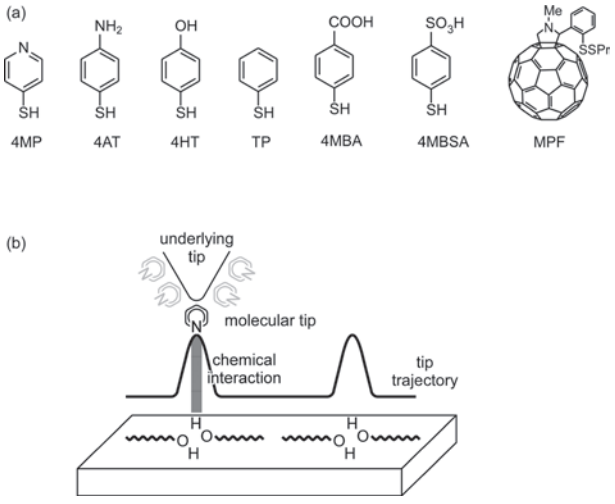

Fig. 1. Molecular tips for selective recognition of functional groups or chemical species. (a) Chemical structures of the molecular tips. Abbreviations: 4MP, 4-mercaptopyridine; 4AT, 4-aminothiophenol; 4HT, 4-hydroxythiophenol; TP, thiophenol; 4MBA, 4-mercaptobenzoic acid; 4MBSA, 4-mercaptobenzenesulfonic acid; MPF, *N*-methyl 2-(2-propyldithiophenyl)fulleropyrrolidine. (b) Schematic illustration of facilitated electron tunneling through a chemical interaction between sample and tip molecules.

2. Interactions for Chemically Selective Imaging

2.1 Charge-transfer interaction[10]

A fullerene molecular tip was used to observe porphyrin molecules adsorbed onto a surface of highly oriented pyro-

lytic graphite (HOPG). Porphyrins are one of the most employed electron donors, and fullerenes possess facile electron acceptability.[11] These two compounds have been known to form a charge-transfer interaction between them[12-14], which leads to formation of supramolecular complexes in solution.[15]

First, a cobalt (II) porphyrin (CoPor, Fig. 2) monolayer was observed to investigate how the fullerene derivative tip affects the tunneling current. Figure 3(a) shows an STM image of the CoPor monolayer observed with a gold tip, in which ordered arrays of porphyrin rings were observed. The porphyrin rings were observed as having central protrusions when gold tips were used as indicated by blue arrows in the STM image [Fig. 3(a)]. The protrusions are assigned to the central cobalt(II) ions, and the large tunneling probability at the cobalt(II) ions has been suggested to result from d-orbital mediated electron tunneling in a resonant way, where the unoccupied orbitals of the half-filled d_{z^2} orbitals coherently couple to the states of the substrate.[16-18] When MPF tips were used and electron tunneling between the single fullerene and individual porphyrin was measured, significantly different images were observed [Fig3(b)]. In strong contrast to Fig. 3(a), the cobalt(II) ions (blue arrows) were observed as depressions, and the pyrrole moieties surrounding them appeared as protrusions, which reveals that the tunnel electrons are localized at the pyrrole moieties. We ascribe the change in image contrast observed with the MPF tips to the charge-transfer interaction concomitant with the overlapped π orbitals between a fullerene moiety of the molecular tip and a pyrrole moiety of the CoPor. The charge-transfer interaction facilitates electron tunneling locally at the pyrrole moiety.

Next, we observed a mixed monolayer of zinc(II) and free-base porphyrins (ZnPor and FBPor, respectively; Fig. 2). Figures 3(c) and 3(d) show STM images of the monolayer observed with a gold and MPF tips, respectively. The sample solution contains two kinds of porphyrins. Nevertheless, the centers of all the porphyrin rings were observed as depressions compared to the surrounding pyrrole moieties in Fig. 3(c). It is natural for the centers of porphyrin rings of FBPor to be observed as depressions because central metal ions are absent in FBPor. The d_{z^2} orbitals of zinc(II) ions in ZnPor are fully filled unlike those of cobalt(II) ions in CoPor, which results in little tunneling current at the central metal ions. This presumably accounts for the depressed appearance of the centers of ZnPor.[16] In addition, all the porphyrin rings were observed as equally bright protrusions in Fig. 3(c), and as a result the two species that should coexist on the surface cannot be discriminated from each other. In contrast to Fig. 3(c), one porphyrin ring was observed much brighter than the other one in Fig. 3(d). A wider image obtained using a MPF tip (75 nm × 75 nm, data not shown) showed 108 and 326 molecules having the brighter and dimmer rings, respectively. Their ratio (108/326 = 1.0/3.0) is in an exact agreement with the molar ratio of ZnPor to FBPor in the sample solution. This suggests that the brighter and dimmer porphyrin rings in Fig. 3(d) correspond to those of ZnPor and FBPor, respectively.[9]

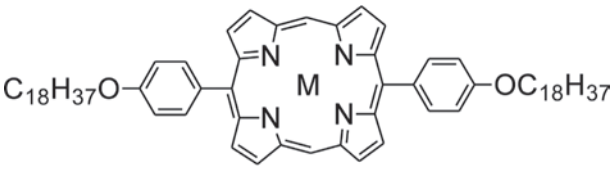

CoPor : M = Co(II)
ZnPor : M = Zn(II)
FBPor : M = 2H (metal free)
NiPor : M = Ni(II)

Fig. 2. Chemical structures of CoPor, ZnPor, FBPor, and NiPor.

The difference in image contrast of FBPor and ZnPor in Fig. 3(d) is ascribed to the differing extent of the charge-transfer interactions of the two kinds of porphyrins with the fullerene tip. The difference in the extent of the charge-transfer interaction is evident by considering the difference in energy between π HOMOs of FBPor and ZnPor. The π HOMO energy of zinc(II) tetraphenylporphyrin is reported to be 0.3 eV above that of the free-base derivative.[16] The zinc(II) derivative is thus expected to have favorable charge-transfer interaction with the fullerene compared with the free-base derivative,[19] because the π HOMO of the former is energetically closer to the LUMO of a fullerene than the latter [Fig. 3(e)]. The favorable charge-transfer interaction between the fullerene and ZnPor facilitates electron tunneling to a great extent compared with the interaction between the fullerene and FBPor, which results in the brighter appearance for ZnPor in Fig. 3(d). These results demonstrate that the localized electron tunneling through charge-transfer interactions can be applied to spatially visualize frontier orbitals involved in the interaction.

2.2 Hydrogen bond interaction[4-8]

It has been well established both experimentally and theoretically that electron tunneling through hydrogen bond interaction plays important roles especially in biological electron-transfer processes.[20] In these processes, hydrogen bond has been shown to strongly mediate elec-

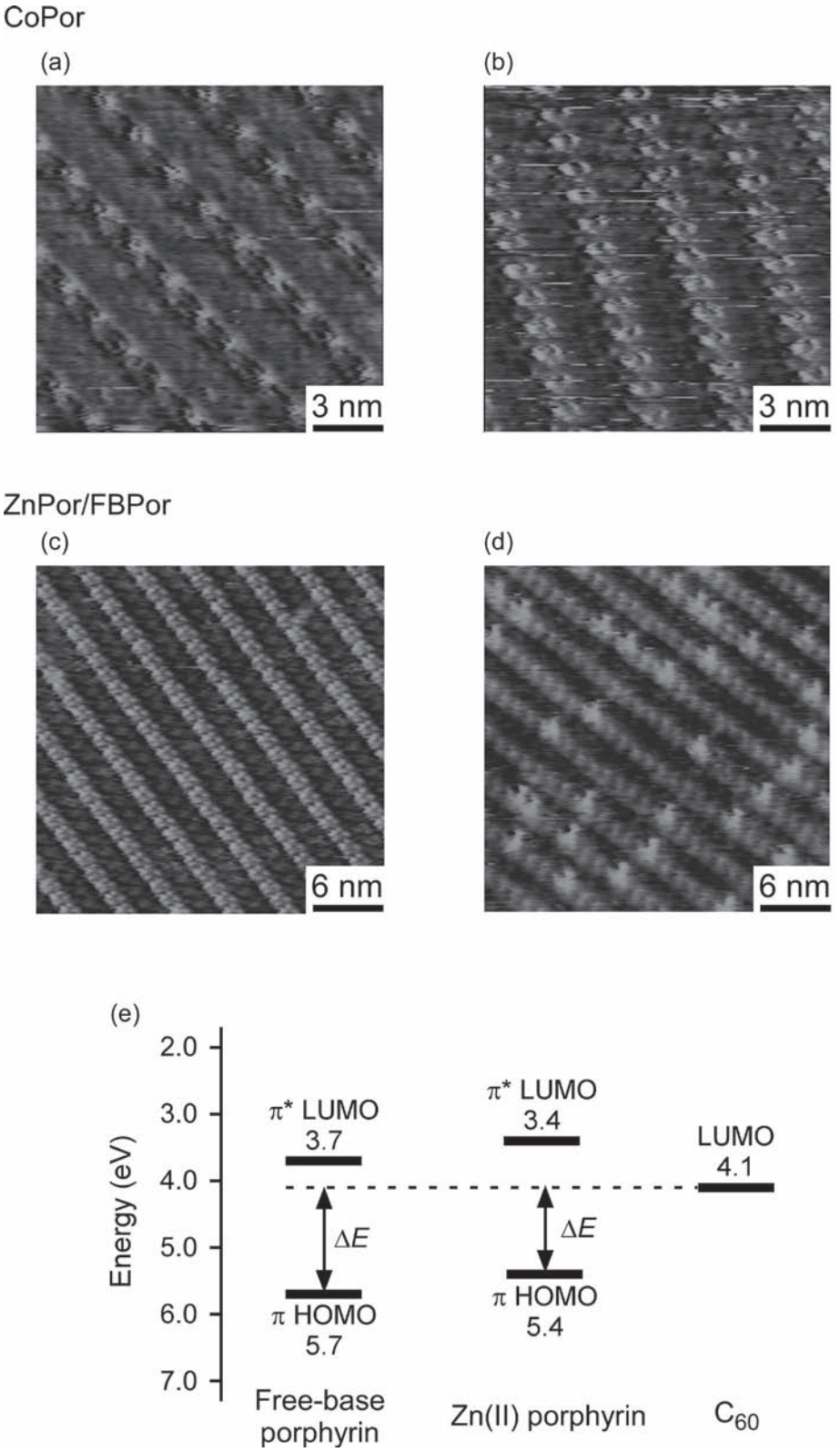

Fig. 3. STM images of the porphyrin monolayers on HOPG. (a) CoPor observed with an unmodified gold tips. Bias voltage, –1.30 V (sample negative); tunneling current, 0.30 nA. (b) CoPor observed with a MPF tip. Bias voltage, –1.25 V; tunneling current 0.30 nA. (c) FBPor and ZnPor observed with an unmodified gold tip. Bias voltage, –1.20 V; tunneling current, 0.35 nA. (d) FBPor and ZnPor observed with a MPF tip. Bias voltage, –1.30 V; tunneling current, 0.45 nA. (e) An energy diagram of free-base and zinc(II) tetraphenylporphyrin (FBTPP and ZnTPP, respectively) and fullerene (C_{60}). All of them are relative to the vacuum level.

tronic coupling between a donor and acceptor, and to reduce the effective tunneling barriers in between.[21] We found that such facilitation of electron tunneling through hydrogen bond interaction also arises with STM molecular tips. Molecular tips thereby allow for selective recognition of a variety of functional groups based on hydrogen bond

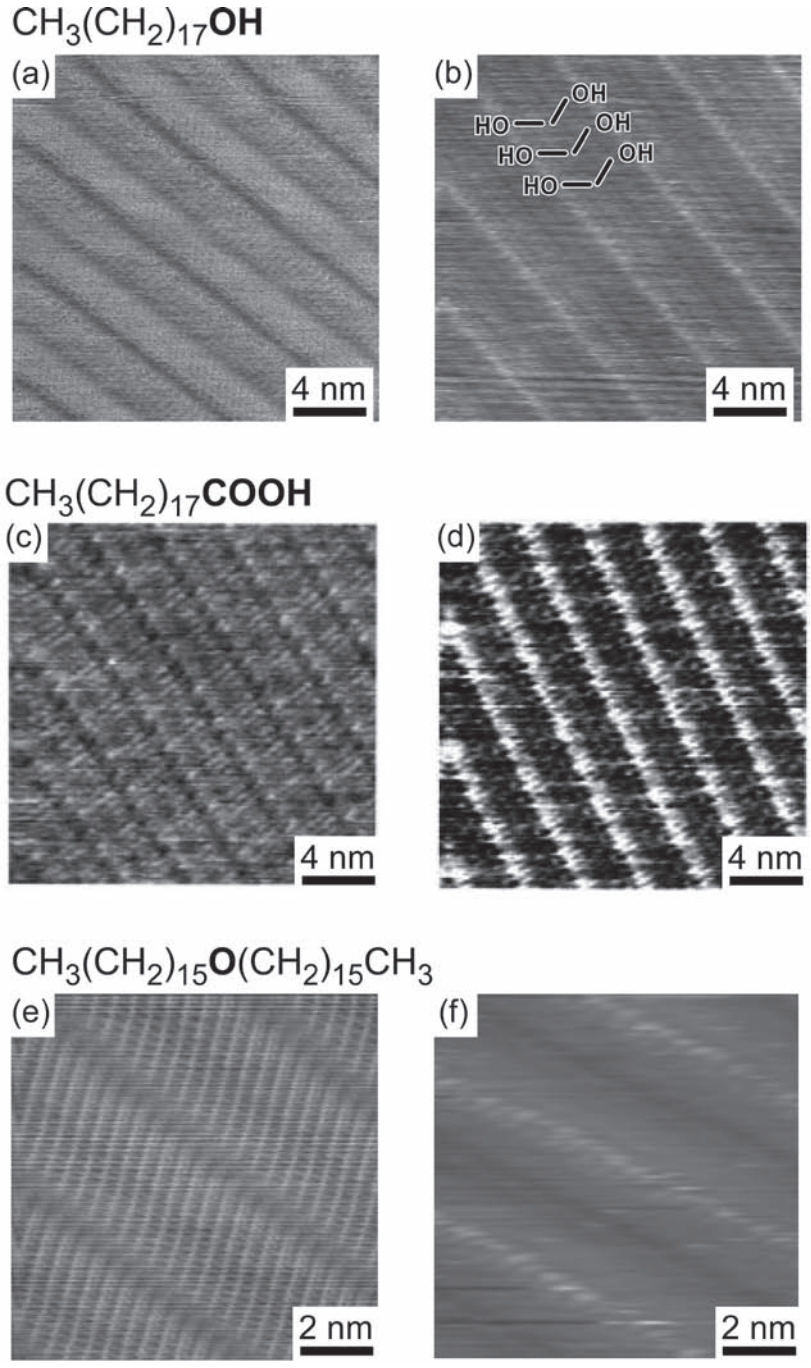

Fig. 4. STM images of substituted hydrocarbons on HOPG. (a) 1-Octadecanol observed with an unmodified gold tip. Bias voltage, –1.0 V (sample negative); tunneling current, 1.0 nA. (b) 1-Octadecanol observed with a 4MP tip. Bias voltage, –1.0 V (sample negative); tunneling current, 0.7 nA. (c) 1-Ocatadecanoic acid observed with an unmodified gold tip. Bias voltage, –0.7 V (sample negative); tunneling current, 0.7 nA. (d) 1-Ocatadecanoic acid observed with a 4MP tip. Bias voltage, +0.4 V (sample positive); tunneling current, 0.7 nA. (e) Dihexadecyl ether observed with an unmodified tip. Bias voltage, –0.90 V (sample negative); tunneling current, 0.70 nA. (f) Dihexadecyl ether observed with a 4MBA tip. Bias voltage, –0.90 V (sample negative); tunneling current, 0.70 nA.

interaction between these functional groups and the tip molecules. The hydrogen bond interaction increases tunneling current at the functional groups, and as a result the functional groups appear as bright protrusions.

Figure 4(a) shows a typical STM image of a 1-octadecanol monolayer observed with unmodified gold tips. Lamella structures consisting of bright parallel bands were observed, each lamella being separated from the adjacent lamellae by dark borderlines. The length of the bright bands was 2.4 ± 0.2 nm, which agrees well with the length of a C_{18} carbon chain in all-*trans* conformation. This indicates that these bands correspond to octadecyl chains physisorbed on the graphite surface. The -OH groups of 1-octadecanol molecules cannot exactly assigned, because the terminal methyl groups are similarly shown as darker parts. In contrast, 4MP tips gave parallel bright lines separated by 4.4 ± 0.2 nm, which almost corresponds to twice the width of the lamella of $C_{18}OH$ and the separation of -OH in the monolayer [Fig. 4(b)]. Similar changes in image contrast were observed with molecular tips having functional groups that can form hydrogen bonds (4AT, 4HT), but were not obtained with TP tips, which has no functional group for hydrogen bond. These results indicate that the contrast changes arise due to the presence of -OH residues of the sample and are due to hydrogen bond interactions between the functional groups on tip and sample.[4] Similarly, carboxy groups[4] [Fig. 4(d)] and ether oxygens[6] [Fig. 4(f)] were selectively observed by 4MP and 4MBA tips, respectively, based on hydrogen bond interactions, whereas these functional groups cannot be recognized with metal tips [Figs. 4(c) and 4(e)]. In the above examples, the molecular tips used for selective recognition of –OH and –COOH groups have hydrogen bond-accepting functional groups, while the 4MBA molecule has hydrogen bond-donating groups. In both cases, increases in the tunneling current were observed, indicating that the direction of hydrogen bond interaction does not affect the facilitation of electron tunneling.

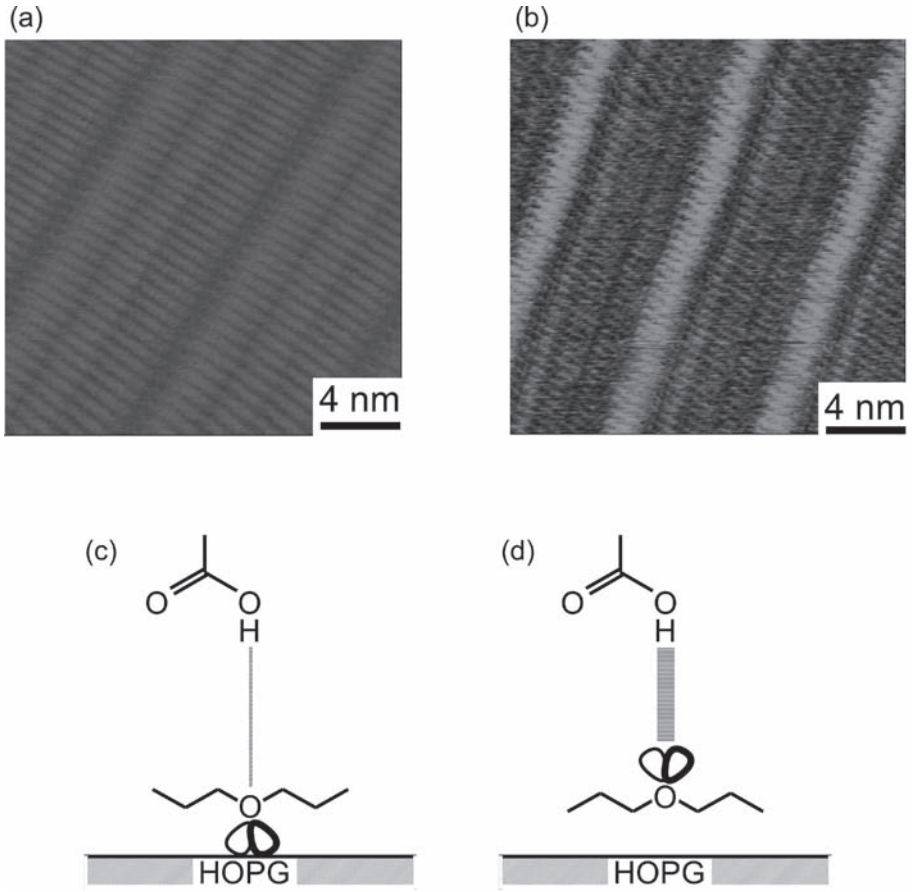

Fig. 5. STM observation of $C_{16}OC_{10}OC_{16}$ on HOPG. (a) STM image of $C_{16}OC_{10}OC_{16}$ observed with an unmodified gold tip. Bias voltage, –1.0 V (sample negative); tunneling current, 0.6 nA. (b) STM image of $C_{16}OC_{10}OC_{16}$ observed with a 4MBA tip. Bias voltage, –0.8 V (sample negative); tunneling current, 0.5 nA. And schematic illustration of the hydrogen bond interactions between carboxy groups of 4MBA and ether oxygens in (c) unfavorable and (d) favorable orientation.

This method was found to discriminate even molecular orientation or conformation of diether, $CH_3(CH_2)_{15}O(CH_2)_{10}O(CH_2)_{15}CH_3$ ($C_{16}OC_{10}OC_{16}$), where the direction of two oxygen lone pairs could be respectively discriminated by 4MBA tips.[7] Figures 5(a) and 5(b) show STM images of $C_{16}OC_{10}OC_{16}$ monolayers observed with an unmodified and a 4MBA-modified tip, respectively. With 4MBA tips pairs of bright lines were observed [Fig. 5(b)]. The separation of two bright lines within the same pair is 2.0 ± 0.3 nm, which is close to 1.4 nm for the estimated length of the alkyl spacer between the two ether oxygen atoms of $C_{16}OC_{10}OC_{16}$. This result further supports the interpretation that the bright lines in the images obtained with tips modified with 4MBA reveal the position of the ether oxygens in the sample molecules. Interestingly, one bright line in a pair is much brighter than the other one in Fig 5(b). CPK models of these diethers in all-*trans* conformation show that the non-bonding oxygen orbitals of $C_{16}OC_{10}OC_{16}$ point in opposite directions. The orbitals of one oxygen point downwards, and the lone-pair orbitals of the second oxygen point upwards. Because the orientation in which the donor and acceptor directly face each other is most favorable for hydrogen bond formation, the oxygen atom with the lone-pair electrons pointing upwards [Fig. 5(c)] can form much stronger hydrogen bonds with 4MBA on the tip than the oxygen with the lone-pair orbitals pointing downwards [Fig. 5(d)]. This difference in the strength of the hydrogen bond causes the difference in the brightness for the two oxygens.

2.3 Metal coordination bond interaction[9]

Coordination-bond-facilitated tunneling was also observed with 4MP tips to discriminate metalloporphyrins (Fig. 2) with different metal centers.[9]

Figure 6(a) shows a typical STM image of a mixed monolayer formed from a solution containing ZnPor and NiPor with a molar ratio of 1.00:0.33, which was observed with a 4MP tip. The central parts of the porphyrins appear as very bright spots and moderately bright spots. Figure 6(a) exhibits 76 very bright spots and 31 moderately bright spots in a scan area of 25 × 25 nm^2, giving a ratio of 1.00:0.41 for the number of very bright spots to that of moderately bright spots, which is close to the molar ratio of the ZnPor to NiPor in the sample solution (ZnPor:NiPor = 1.00:0.33). With increasing concentration of ZnPor in the ZnPor/NiPor solution, the number of very bright spots increased [Fig. 6(b)]. Upon a decrease in the concentration of ZnPor in the ZnPor/NiPor solution, the number of very bright spots decreased [Fig. 6(c)]. This indicates that very bright spots are of the ZnPor and moderately bright spots are the NiPor centers. When STM measurements were performed with unmodified and TP tips, the all porphyrin centers in the same mixed monolayer appeared as dark

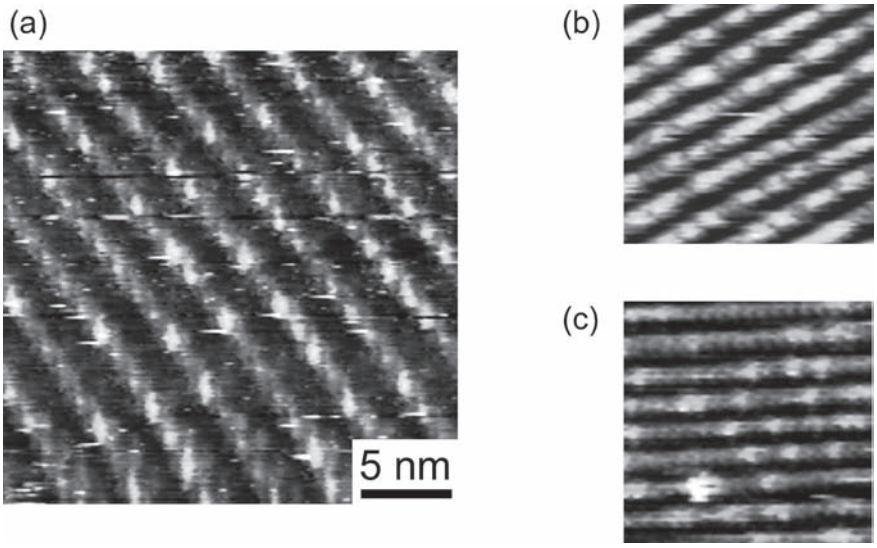

Fig. 6. (a) STM image of a mixed monolayer of ZnPor and NiPor (molar ratio of ZnPor and NiPor in the sample solution; ZnPor: NiPor = 1.00:0.33) with a 4MP tip. Bias voltage, –1149 mV (sample negative); tunneling current, 322 pA. (b) STM image of a mixed monolayer of ZnPor and NiPor (molar ratio of ZnPor and NiPor in the sample solution; ZnPor:NiPor = 1.00:0.20). Bias voltage, –1327 mV (sample negative); tunneling current, 440 pA. (c) STM image of a mixed monolayer of ZnPor and NiPor (molar ratio of ZnPor and NiPor in the sample solution; ZnPor:NiPor = 1.0:5.0). Bias voltage, –1148 mV (sample negative); tunneling current, 524 pA, range of vertical height in the image, 0.5 nm.

depressions and the two types of porphyrins were unable to be distinguished.

Because selective contrasts at porphyrin centers in images with 4MP were observed at the metal centers of ZnPor and NiPor, they were most probably induced by the metal coordination interactions between the pyridyl group of 4MP and central metals of the porphyrins. Indeed, the stabilities of axial complexes of zinc(II) porphyrins are fairly high (e.g., $K = 10^3$–10^5 M^{-1} for pyridine or piperidine in benzene or toluene as solvents[22]), and nickel(II) porphyrins also bind one or even two axial ligands (e.g., $K_1 = 0.4$ M^{-1}, $K_2 = 2.5$ M^{-1} for axial complexation between nickel(II) tetraphenyloxyporphyrin and pyrrolidine in dichloromethane[23]). The involvement of metal coordination interactions in the contrast changes is probably supported by the correlation between the stability of the axial complexes for zinc(II) and nickel(II) porphyrins and the extent of the contrast change.

3. Control of Chemical Selectivity[24]

We have studied how hydrogen bond acidity or basicity of the tip molecule affects the increase in the tunneling current for oxygen-containing functional groups of sample. Three kinds of molecular tips (4MP, 4MBSA, and 4MBA) were used for the STM observation of behenic acid 16-hydroxyhexadecyl ester ($CH_3(CH_2)_{20}COO(CH_2)_{16}OH$, abbreviated hereafter as $C_{21}COOC_{16}OH$). The TP contains no functional group for hydrogen bond formation, and the 4MP has a pyridine group, which can work only as a hydrogen bond acceptor. The sulfonyl group of 4MBSA and the carboxy group of 4MBA can form hydrogen bond as donors, but differ in hydrogen bond acidity from each other.

Figure 7(a) shows a typical STM image of a $C_{21}COOC_{16}OH$ monolayer observed with an unmodified gold tip. A lamella structure was seen, and the lamellae were separated from each other by wide and narrow dark lines. The terminal hydroxy groups, which should correspond to either wide or narrow dark lines in Fig. 7(a), cannot be specified as reported previously.[4, 5] The alternate appearance of the wide and narrow dark lines suggests that the sample molecules adsorb onto HOPG with their hydroxy groups head-to-head as illustrated in Fig. 7(b). No additional distinct bright or dark lines were observed in Fig. 7(a), and it is consequently difficult to discriminate the carboxylate moieties of $C_{21}COOC_{16}OH$ from the alkyl residues.

When 4MP-modified tips were used for the observation of a $C_{21}COOC_{16}OH$ monolayer, parallel bright lines were observed [Fig. 7(c)]. Based on the previous result (see above), it can be concluded that the bright lines reveal the positions of the hydroxy groups of $C_{21}COOC_{16}OH$. The pyridine nitrogen of the 4MP SAMs on the tip can form hydrogen bonds only with a hydrogen-bond donor, and thus, they can interact only with the hydroxy groups of the sample. The changes in image contrast selective to the hydroxy groups in Fig. 7(c) can be explained by this selective hydrogen bond interaction with the pyridine of 4MP-SAMs on the tip, which probably enhances tunneling probability.[4]

Figure 7(d) presents an STM image of a $C_{21}COOC_{16}OH$ monolayer observed with a 4MBSA-modified tip. In this image, a set of three bright lines, which consists of a single narrower bright line and neighboring two wider bright lines, was observed. From geometrical considerations, it was concluded that the central narrower bright lines correspond to the hydroxy groups, and the outer two bright lines to the carboxylate moieties of $C_{22}COOC_{16}OH$. The dark lines locating approximately at the middle of two neighboring wider bright lines (white arrows) are attributed to the intermolecular troughs between the adjacent lamellae. Next, 4MBA molecular tips were used for the STM observation of $C_{21}COOC_{16}OH$ monolayers. In the STM image [Fig. 7(e)], bright single lines were observed like the image observed with 4MP tips [Fig. 7(c)], and the bright lines were assigned to the hydroxy groups of the $C_{21}COOC_{16}OH$ molecules. Interestingly, 4MBA-modified tips unlike 4MBSA-modified tips exhibited no discernible bright lines that can be attributed to the presence of the carboxylate. Because both the sulfonyl group of 4MBSA and the carboxy group of 4MBA can be hydrogen bond donors, they can interact with hydrogen bond acceptors. In the STM image of $C_{21}COOC_{16}OH$ observed with 4MBSA-modified tips, a set of three bright lines was observed, revealing both positions of the hydroxy and of the carboxylate moieties of the sample molecules [Fig. 7(d)]. In contrast, with 4MBA-modified tips, only a single bright line that corresponds to the hydroxy group was observed. The presence and absence of the contrast enhancement on carboxylate moiety in Figs. 7(d) and 7(e), respectively, can be explained on the basis of the differing extent of the hydrogen bond interaction. Hydrogen bond interactions of the carboxylate moiety are much weaker with the carboxy group of 4MBA-modified tips than with the sulfonyl group of 4MBSA-modified tips, because the hydrogen bond acidity of carboxy groups is in general much lower than that of

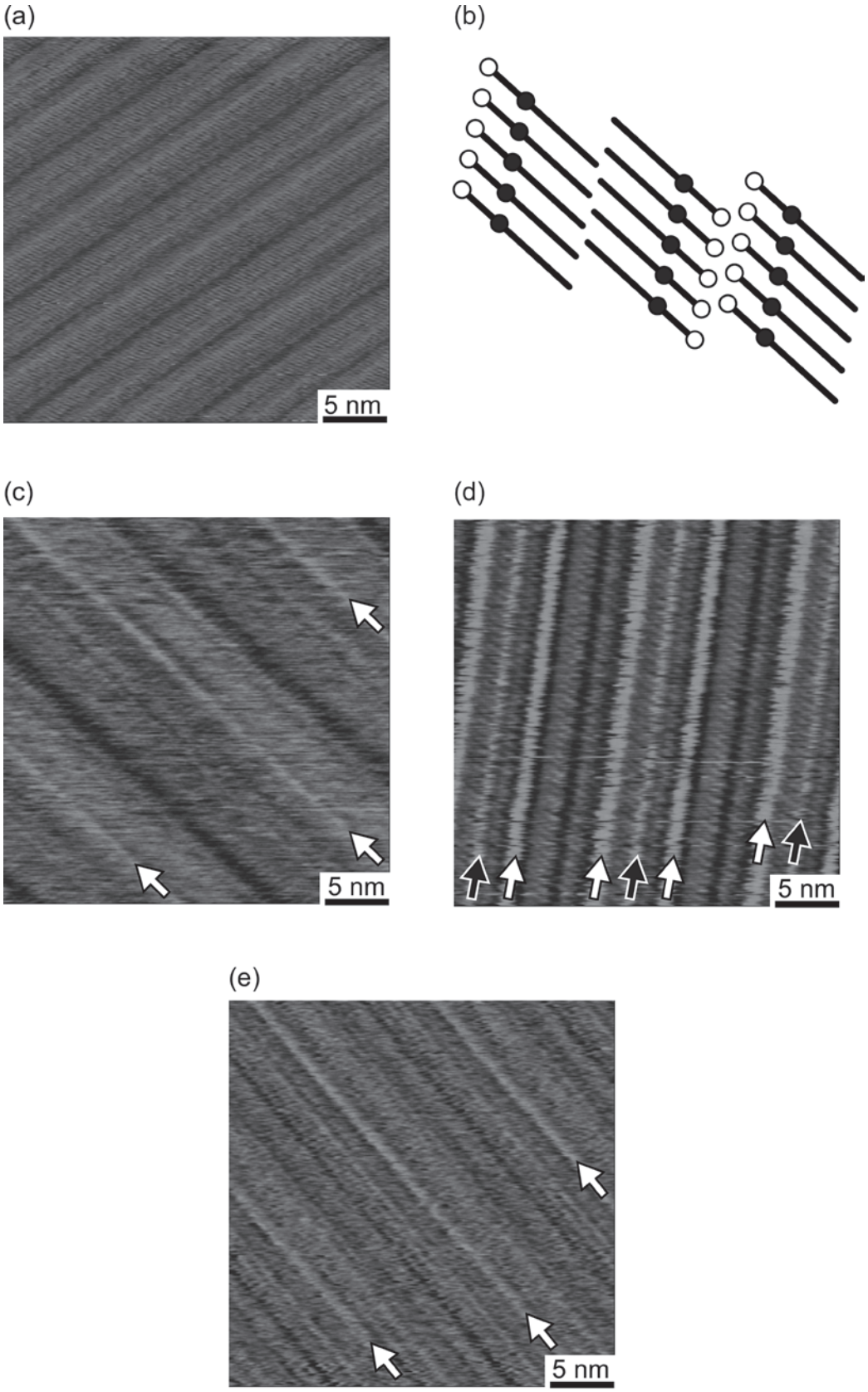

Fig. 7. STM images of $C_{21}COOC_{16}OH$ observed (a) with an unmodified gold tip, (c) with a 4MP tip, (d) with a 4MBSA tip, and (e) with a 4MBA tip. Bias voltage, –1.0 V (sample negative); tunneling current, 0.5 nA. Arrows point the bright lines that appeared by using the molecular tips. The molecular arrangement of the adsorbed molecules is schematically shown in (b).

sulfonyl groups. On the other hand, hydrogen bond basicity of the hydroxy group is almost the same as that of the carboxylate moiety in nonpolar solvents.[25] However, 4MBA-modified tips gave the contrast change only selective to the hydroxy group. Because the carboxy groups of 4MBA SAMs on the tip can be both of hydrogen-bond acceptor and donor, this result seems to reflect the hydrogen bond acidity of the hydroxy groups. Owing to the acidity, the carboxy group of 4MBA SAMs on the tip is subject to stronger hydrogen bond interaction with the hydroxy group than with the carboxylate moiety in the sample molecule. Hydrogen bond interaction between the carboxy group of 4MBA and the carboxylate moiety of the sample may not be strong enough to enhance the tunneling current. These results indicate chemical selectivity can be controlled by changing the hydrogen bond strength through the design of the tip functionality.

4. Discrimination of DNA Nucleobases[26]

Very recently, we showed that a nucleobase molecular tip is capable of electrically pinpointing each complementary nucleobase. The nucleobase molecular tips were prepared by chemical modification of underlying metal tips with thiol derivatives of adenine, guanine, cytosine, and uracil (Fig. 8). Figures 9(a), (b), and (c) show typical STM images of guanine SAMs observed with complementary cytosine, noncomplementary adenine, and unmodified tips, respectively. Cross sectional profiles of the images are shown in Fig. 9(d), which represents the extent of electron tunneling between the tip and nucleobase. The complementary cytosine tip exhibited the most facilitated electron tunneling and therefore the brightest guanine images among the three tips. Similarly, for adenine, cytosine, and uracil, their complementary nucleobase tips gave the brightest images of their counterparts, the results of which are shown in Fig. 9(e) together with those using irrelevant tips for validation. Taken together, it is concluded that the complementary combinations of the tip and sample base pairs facilitated the largest electron tunneling through hydrogen bonds between complementary base pairs, and particular nucleobases were thus discriminated from other nucleobases in STM images by using the complementary nucleobase tips.

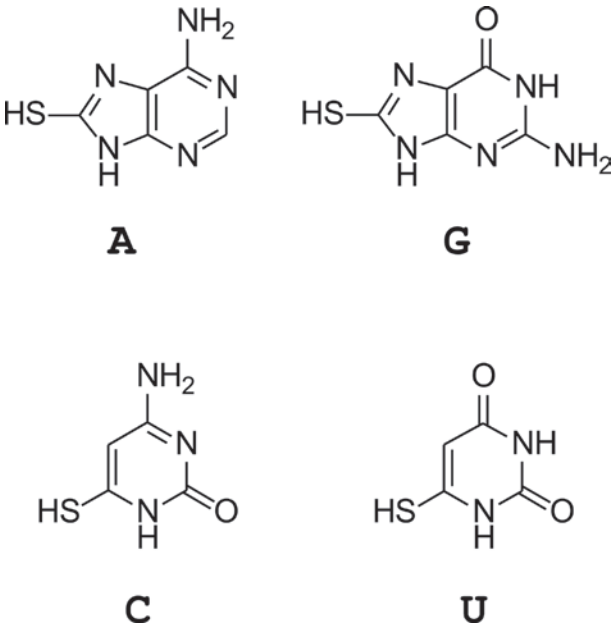

Fig. 8. Chemical structures of thiolated nucleobases employed as molecular tips.

It should be noted that formations of the specific hydrogen bonds between complementary bases require coplanar configurations, in which the molecular planes of the sample and tip nucleobases coincide with each other. The selective large facilitation observed with complementary base pairs on a tip and substrate indicates that the base–base coplanar orientation was in fact achieved. The base–base coplanarity is probably attained by the rotation of a carbon–sulfur bond in the thiolated nucleobase on a tip, which is well known even in the close-packed structure of alkanethiolate SAMs.[27]

An example of the detection of particular nucleobases was demonstrated here with the present method in an 18-mer strand of a peptide nucleic acid (PNA), an analogue of DNA.[28] A typical STM image with an unmodified tip of a PNA strand is shown in Fig. 10(a), showing that bases in the strand were observed as rows of bright spots and the components of the strand, guanines and thymines, were not discriminated. On the contrary, cytosine tips pinpointed the complementary guanines among the noncomplementary thymines in the strands [Fig. 10(b)–(d) and Insets]. The extent of electron tunneling along the strands shows that a single- and double-base substitution in the strands was distinguished with the cytosine tip.

5. Conclusions

We described our studies on molecular STM tips. When molecular tips were used for imaging, a tunneling current increased at specific functional groups and chemical species on the basis of hydrogen bond, metal coordination bond, and charge transfer interactions. As a result, we can determine not only the distribution of the specific functional groups and chemical species but also the orientation of functional groups. In addition, nucleobase molecular tip

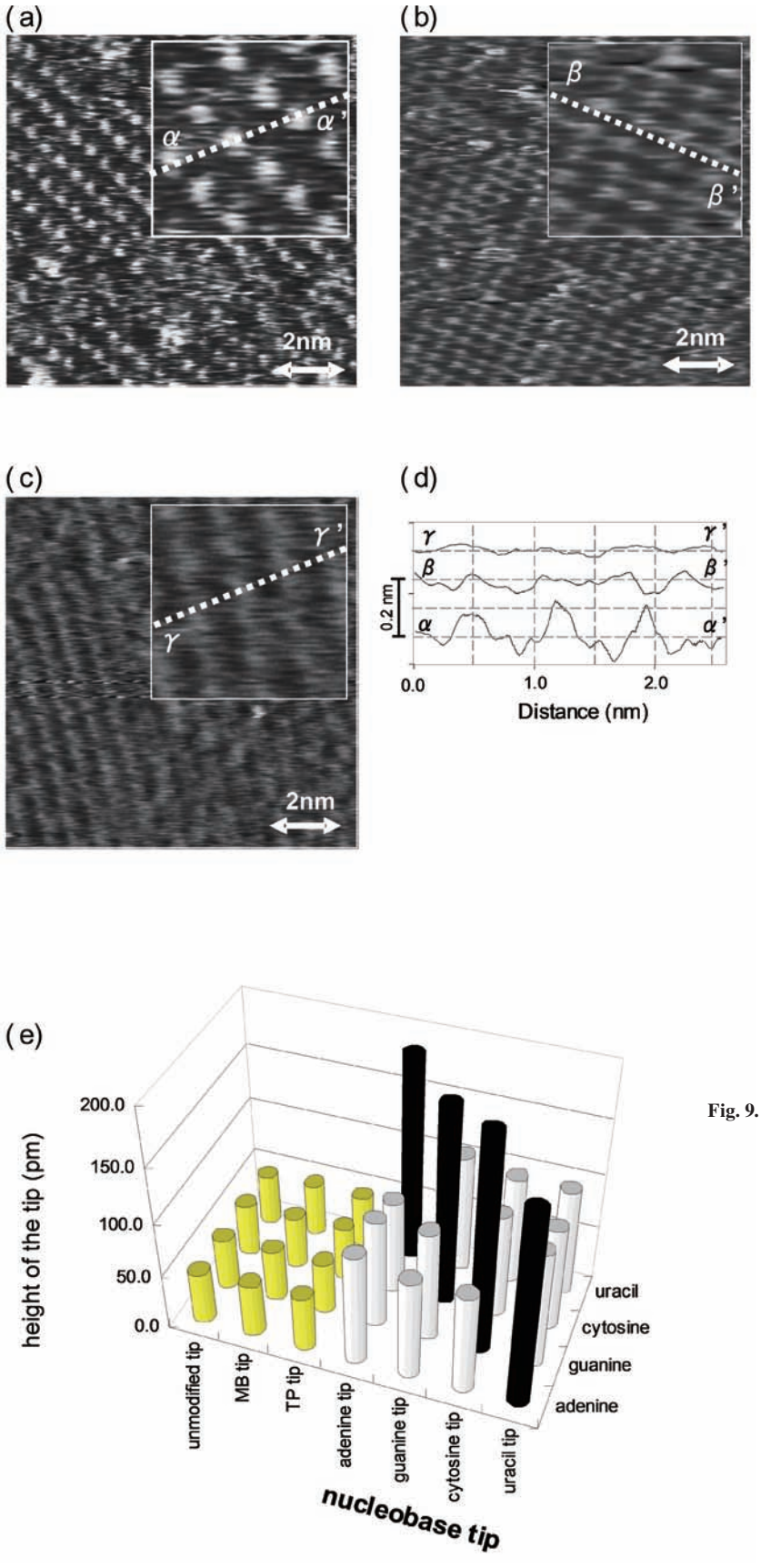

Fig. 9. Changes in the image contrast for guanines; comparison with unmodified, non-complementary, and complementary nucleobase tips. STM image of guanines observed (a) with a complementary cytosine tip, (b) with a non-complementary adenine tip, and (c) with an unmodified tip. The magnified images (2.5 × 2.5 nm^2) of image a, b, and c are shown in the insets, respectively. (d) Cross-sectional profiles along the dashed lines (α-α', β-β', and γ-γ') in the inset of (a), (b), and (c), respectively. (e) Extents of electron tunneling between tip and sample nucleobases. The mean values (n = 10) of the extents of the observed electron tunneling between nucleobase tips (i.e., adenine, guanine, cytosine, and uracil tips) and sample nucleobases (i.e., adenine, guanine, cytosine, and uracil) represented in "height (pm)" of the tips (see image d caption). Those with irrelevant tips (i.e., unmodified, 2-mercaptobenzimidazole, and TP tips) were also obtained, for comparison, under otherwise identical conditions.

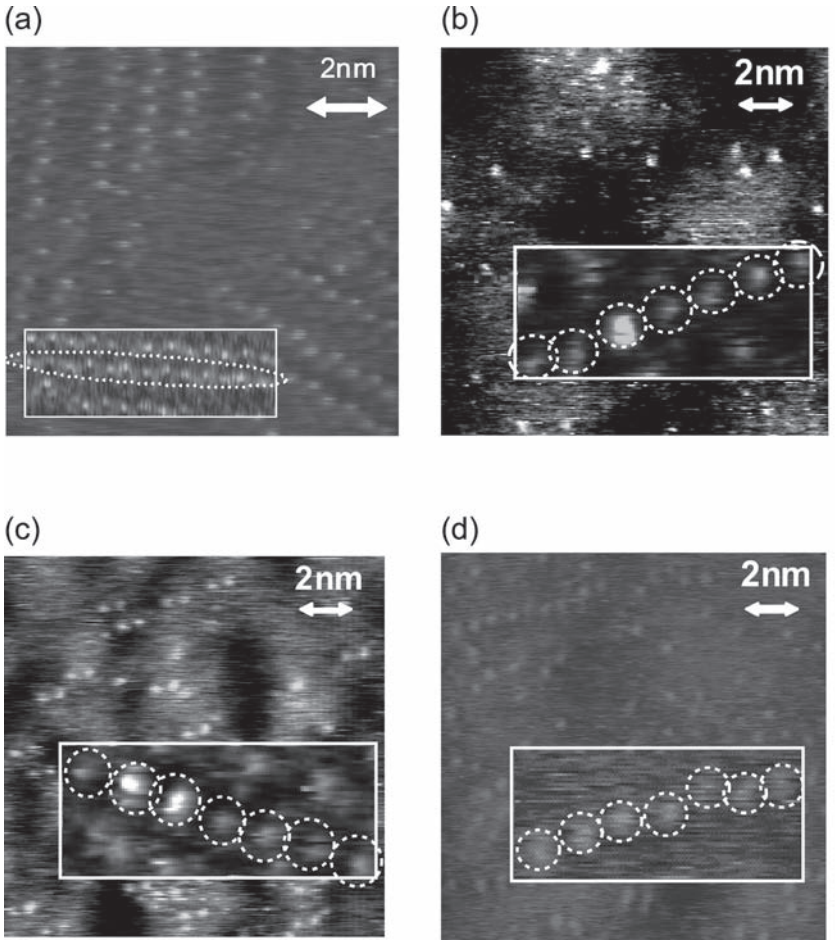

Fig. 10. SNP typing in 18-mer single stranded peptide nucleic acids. (a) An STM image (10 × 10 nm^2) with an unmodified tip of single stranded eighteen-mer PNAs, the sequence of which is TTTTTTTGGTTTTTTTTT. STM images (15 × 15 nm^2) with cytosine tips of three kinds of PNA strands; (b) TTTTTTTTGTTTTTTTTT, (c) TTTTTTTGGTTTTTTTTT, and (d) TTTTTTTTTTTTTTTTTT The magnified images (2.0 × 5.0 nm^2) of image b, c, and d are shown in the insets.

was capable of electrically pinpointing each complementary nucleobase. This technique may be coined "intermolecular tunneling microscopy" as its principle goes, and is of general significance for novel molecular imaging of chemical identities at the membrane and solid surfaces. More sophisticated discrimination of molecular species, such as chiral recognition, may be possible by a rational design of a molecular tip that forms, for example, multiple interactions with the sample molecules.

References

1) R. Wiesendanger, *Scanning Probe Microscopy and Spectroscopy: Methods and Applications.* (University Press, New York, 1994).
2) J. Frommer: Angew. Chem., Int. Ed. Engl. **31** (1992) 1298.
3) L.C. Giancarlo, G.W. Flynn: Annu. Rev. Phys. Chem. **49** (1998) 297.
4) T. Ito, P. Bühlmann, Y. Umezawa: Anal. Chem. **70** (1998) 255.
5) T. Ito, P. Bühlmann, Y. Umezawa: Anal. Chem. **71** (1999) 1699.
6) T. Nishino, P. Bühlmann, T. Ito, Y. Umezawa: Phys. Chem. Chem. Phys. **3** (2001) 1867.
7) T. Nishino, P. Bühlmann, T. Ito, Y. Umezawa: Surf. Sci. **490** (2001) L579.
8) T. Nishino, T. Ito, Y. Umezawa: Anal. Chem. **74** (2002) 4275.
9) T. Ohshiro, T. Ito, P. Bühlmann, Y. Umezawa: Anal. Chem. **73** (2001) 878.
10) T. Nishino, T. Ito, Y. Umezawa: Proc. Natl. Acad. Sci, USA **102** (2005) 5659.
11) H. Imahori, Y. Sakata: Eur. J. Org. Chem. (1999) 2445.
12) P.D.W. Boyd, M.C. Hodgson, C.E.F. Rickard, A.G.

Oliver, L. Chaker, P.J. Brothers, R.D. Bolskar, F.S. Tham, C.A. Reed: J. Am. Chem. Soc. **121** (1999) 10487.
13) D.M. Guldi, C. Luo, M. Prato, E. Dietel, A. Hirsch: Chem. Commun. (2000) 373.
14) D.M. Guldi, C. Luo, M. Prato, A. Troisi, F. Zerbetto, M. Scheloske, E. Dietel, W. Bauer, A. Hirsch: J. Am. Chem. Soc. **123** (2001) 9166.
15) F. Diederich, M. Gómez-López: Chem. Soc. Rev. **28** (1999) 263.
16) L. Scudiero, D.E. Barlow, U. Mazur, K.W. Hipps: J. Am. Chem. Soc. **123** (2001) 4073.
17) L. Scudiero, D.E. Barlow, K.W. Hipps: J. Phys. Chem. B **104** (2000) 11899.
18) D. Barlow, K.W. Hipps: J. Phys. Chem. B **104** (2000) 2444.
19) Y.-B. Wang, Z. Lin: J. Am. Chem. Soc. **125** (2003) 6072.
20) A.M. Kuznetsov, J. Ulstrup, *Electron transfer in chemistry and biology.* (Wiley, New York, 1999).
21) H.B. Gray, J.R. Winkler: Proc. Natl. Acad. Sci, USA **102** (2005) 3534.
22) J.W. Buchler, *Porphyrins and Metalloporphyrins*. (Elsevier, Amsterdam, 1975).
23) K.M. Kadish, K.M. Smith, R. Guilard, *The Porphyrin Handbook: Inorganic Organometallic and Coordination Chemistry.* (Academic Press, New York, 2000).
24) T. Nishino, T. Ito, Y. Umezawa: J. Electroanal. Chem. **550-551** (2003) 125.
25) M.H. Abraham, J.A. Platts: J. Org. Chem. **66** (2001) 3484.
26) T. Ohshiro, Y. Umezawa: Proc. Natl. Acad. Sci, USA **103** (2006) 10.
27) A. Ulman: Chem. Rev. **96** (1996) 1533.
28) P.E. Nielsen, M. Egholm, R.H. Berg, O. Buchardt: Science **254** (1991) 1497.